Since January 2020 Elsevier has created a COVID-19 resource centre with free information in English and Mandarin on the novel coronavirus COVID-19. The COVID-19 resource centre is hosted on Elsevier Connect, the company's public news and information website.

Journal of Colloid and Interface Science 630 (2023) 1–10

Contents lists available at ScienceDirect

Journal of Colloid and Interface Science

journal homepage: www.elsevier.com/locate/jcis

Employing functionalized graphene quantum dots to combat coronavirus and enterovirus

Chien-Te Hsieh [a,b,*], Siyong Gu [c], Yasser Ashraf Gandomi [d], Chun-Chieh Fu [e,f], Po-Yu Sung [a], Ruey-Shin Juang [e,g,h,*], Cheng-Cheung Chen [i,j,*]

[a] Department of Chemical Engineering and Materials Science, Yuan Ze University, Taoyuan 32003, Taiwan
[b] Department of Mechanical, Aerospace, and Biomedical Engineering, University of Tennessee, Knoxville, TN 37996, United States
[c] Fujian Provincial Key Laboratory of Functional Materials and Applications, School of Materials Science and Engineering, Xiamen University of Technology, Xiamen 361024, China
[d] Department of Chemical Engineering, Massachusetts Institute of Technology, Cambridge, MA 02142, United States
[e] Department of Chemical and Materials Engineering, Chang Gung University, Guishan, Taoyuan 33302, Taiwan
[f] Research and Development Division, Gold Carbon Co., Ltd., Taoyuan 320675, Taiwan
[g] Division of Nephrology, Department of Internal Medicine, Chang Gung Memorial Hospital, Linkou, Taiwan
[h] Department of Safety, Health and Environmental Engineering, Ming Chi University of Technology, Taishan, New Taipei City 24301, Taiwan
[i] Institute of Preventive Medicine, National Defense Medical Center, New Taipei City 23742, Taiwan
[j] Graduate Institute of Medical Science, National Defense Medical Center, Taipei City 11490, Taiwan

GRAPHICAL ABSTRACT

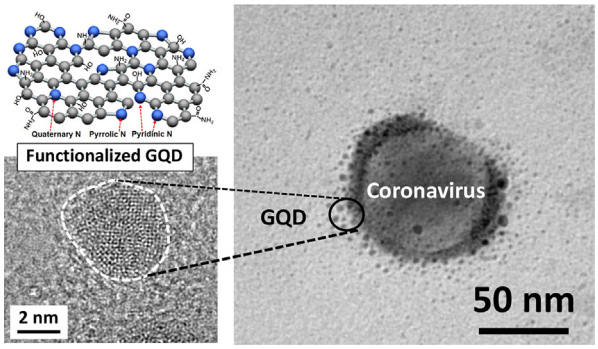

ARTICLE INFO

Article history:
Received 7 March 2022
Revised 11 October 2022
Accepted 16 October 2022
Available online 19 October 2022

Keywords:
Coronavirus deactivation
Enterovirus
Graphene quantum dots
Surface functionality
Solid-phase microwave-assisted method

ABSTRACT

The ongoing COVID-19 (i.e., coronavirus) pandemic continues to adversely affect the human life, economy, and the world's ecosystem. Although significant progress has been made in developing antiviral materials for the coronavirus, much more work is still needed. In this work, *N*-functionalized graphene quantum dots (GQDs) were designed and synthesized as the antiviral nanomaterial for *Feline Coronavirus NTU156* (FCoV NTU156) and *Enterovirus 71* (EV71)) with ultra-high inhibition (>99.9%). To prepare the GQD samples, a unique solid-phase microwave-assisted technique was developed and the cell toxicity was established on the H171 and H184 cell lines after 72 h incubation, indicating superior biocompatibility. The surface functionality of GQDs (i.e., the phenolic and amino groups) plays a vital role in interacting with the receptor-binding-domain of the spike protein. It was also found that the addition of polyethylene glycol is advantageous for the dispersion and the adsorption of functionalized GQDs onto the virus surface, leading to an enhanced virus inhibition. The functionality of as-prepared GQD

* Corresponding authors at: Department of Chemical Engineering and Materials Science, Yuan Ze University, Taoyuan 32003, Taiwan (C.-T. Hsieh). Department of Chemical and Materials Engineering, Chang Gung University, Guishan, Taoyuan 33302, Taiwan (R.-S. Juang). Institute of Preventive Medicine, National Defense Medical Center, New Taipei City 23742, Taiwan (C.-C. Chen).
E-mail addresses: cthsieh@saturn.yzu.edu.tw (C.-T. Hsieh), rsjuang@mail.cgu.edu.tw (R.-S. Juang), chengcheung_chen@gapps.ndmctsgh.edu.tw (C.-C. Chen).

https://doi.org/10.1016/j.jcis.2022.10.082

nanomaterials was further confirmed where a functionalized GQD-coated glass was shown to be extremely effective in hindering the virus spread for a relatively long period (>20 h).

1. Introduction

The eradication of viral infections is an ongoing challenge worldwide, not only due to its ultra-fast spreading but also because of the virus's ability to escape the therapy by genetic mutations [1]. On 30 January 2020, novel coronavirus pneumonia pandemic was declared as "public-health emergency of international concern" by the World Health Organization [2]. So far, the world is still facing the potential catastrophe of a global pandemic due to the rapid surge in the number of people being infected with the novel human coronavirus (i.e., severe acute respiratory syndrome coronavirus 2 (SARS-CoV-2)) leaving the world in dire need of possible cure regimens and effective therapies [3,4]. The structure of coronavirus generally consists of a single-stranded positive-sense ribonucleic acid (RNA) with ~ 30,000 nucleotides. Besides, the coronavirus contains five structural proteins, namely, (i) spike (S), (ii) nucleocapsid, (iii) envelope, (iv) membrane, and (v) hemagglutinin esterase dimer [5]. Predominantly, the S protein (i.e., spike protein) plays a vital role in infecting cells by determining the host antibodies and neutralizing them [6]. The S protein of the recent coronavirus (e.g., SARS-CoV-2) encompasses two subunits (S1 and S2), where the receptor-binding-domain (RBD) within S1 subunit joins to the human angiotensin-converting enzyme 2 (ACE2) receptor (dimer) [7]. This is primarily due to the S protein's strong affinity toward human receptor ACE2 upon entering the host cells [8], where ACE2 is an enzyme attached to the cell membranes of the lower respiratory tract of lungs, stomach, small intestines, colon, kidney, lymph nodes, and liver bile ducts [4,9]. As a result, the ACE2 is usually considered a major entry point for the coronavirus.

To find effective therapeutics, viral entry, mode of attachment, and replication are the key parameters to be assessed for the intervention strategies [3]. The antiviral agents are categorized into the virucidal (they destroy the supercritical membrane and the virion protein capsid or penetrate into the virion and damage the viral genome irreversibly) and the virustatic (These substances reversibly interact with the virus where some parameters like pH, temperature, and dilution can cause the release of virions) [10–12].

Recently, nanoscale materials have appeared as promising and efficient platforms to modulate the viral infection cycle. Being relatively inexpensive with unique physicochemical properties, the graphene quantum dots (GQDs) are emerging class of antiviral nanomaterials [3]. Detailed analysis has shown that various CQDs are an excellent photodynamic antibacterial agent for treatment of bacterial infections [13–16]. Main mechanisms of bacteria death caused by GO are: membrane rupture and production of reactive oxygen species (ROS) [17–19]. Basically, the GQDs are ultra-small pieces of graphene (particle sizes range: 3–20 nm) consisting of no>5 layers of graphene layers (~2.5 nm) [20,21]. Thanks to their tunable semiconducting characteristics, GQDs have been employed within the optical and bio-imaging probes [22–25], metal-free catalysts [26,27], and energy-storage materials [28–32]. Compared to other metal-oxide quantum dots, GQDs have attracted considerable attention because of their excellent biocompatibility, nontoxicity, facile modification capability, robust chemical inertness, high solubility (in aqueous solutions), and environmental friendliness [32]. Given that the attachment of viruses to the host cells is favored by multivalent interactions, GQDs can be chemically functionalized via implementing various surface functionalities on the basal plane or on the edge sites. Indeed, the multivalent characteristics of the GQDs along with their intrinsic high surface to volume ratio, enables the attachment of various ligands. Therefore, the functionalized GQDs can potentially hinder the viral entry into cells.

Pioneering studies have reported on triggering the antiviral properties of GQDs via the heteroatom doping [1]. The synergy between co-doping of GQDs and the surface-functionalized triazole derivatives can be extremely effective in generating potential antiviral candidates, capable of operating either via signal transduction or cytosolic protein interactions [33]. Considering the promising properties of GQDs, potential applications of these nanomaterials for combating the coronavirus spread (e.g., SARS-CoV-2) requires more thorough investigation. Understanding the receptor recognition mechanism of the coronaviruses and their binding with the substrate pocket of the host cell is essential in elucidating the inhibitory mechanism of the amine-functionalized GQDs [34]. Herein, unleashing potential antiviral attributes of GQDs can bring significant attention to these finely tuned nanomaterials in combatting the coronaviruses' spread. However, to the best of our knowledge, there are no prior efforts on systematic investigation of antiviral properties of *N*-functionalized GQDs for the coronavirus.

In this work, we have doped GQDs with heteroatoms to enable in-plane substitution of N atoms and to decorate *N*-containing functionalities. The as-prepared GQDs are indeed *n*-type semiconductive materials. An efficient solid-phase microwave-assisted (SPMA) technique was employed for synthesizing highly-amidized GQDs, where the carbon to nitrogen precursor was chosen to adjust the amidation level of the resulting GQDs [35,36]. The functionalized GQDs prepared in this study can be used to combat two kinds of viruses including *Feline Coronavirus NTU156* (FCoV NTU156) and *Enterovirus 71* (EV71). FCoV NTU156 is a positive-sense, single-stranded RNA virus with a lipid envelope and belongs to the *Coronaviridae* family [37], whereas the EV71 is considered a member of the genus Enterovirus from the *Picornaviridae* group [38]. We have also demonstrated how the nitrogen functionalities improve the antiviral effect of as-synthesized GQDs for the coronavirus. Finally, one strategy to prepare antiviral GQD surfaces as viral inhibitors against coronavirus has been proposed.

2. Experimental

2.1. SPMA synthesis of functionalized GQDs

The SPMA technique was adopted for preparing the GQD samples where a home-made microwave reactor (volume: 60 L), equipped with an efficient microwave emitter (nominal power: 6 kW), and a rotary sample plate were employed for the synthesis. The reactor could accommodate six reaction tubes (diameter: 150 mm; height: 60 mm) simultaneously under microwave irradiation. First, two kinds of precursors, citric acid ($C_6H_8O_7$, molecular weight: 180, purity: 99%, Showa) and urea (CON_2H_4, molecular weight: 60, purity: 99%, Avantor) were uniformly mixed in a 2D mixer at 500 rpm using Zr balls for 30 min. Three GQD configurations (*ca.* 80 g) with different ratios of citric acid to urea (1/3, 1/1, and 3/1 in w/w) were prepared and placed on the sample plate with the rotational speed of 60 rpm. The solid mixture of citric acid and urea was heated under the microwave irradiation at 280 °C

[35,36]. The SMPA method was carried out in air atmosphere and resulted in a high production yield of ~ 40 wt%. Subsequently, the GQD powders were ball-milled and then were sieved through a 200-mesh metallic screen. Followingly, the solid precipitate was dispersed and washed using ultrapure water. Finally, the powders were centrifuged and collected at 10,000 rpm for 30 min to remove the residual precursors. The as-prepared GQD samples were labeled as GQD-1 (weight ratio of citric acid/urea: 1/3), GQD-2 (1/1), and GQD-3 (3/1).

2.2. Materials characterization of functionalized GQDs

A high-resolution transmission electron microscope (HR-TEM, FEI Talos F200s) operating at 200 kV was used to record the micrographs. The procedure concerning the sample preparation was briefly described in the ***Electronic*** ***Supporting Information*** (S1.1). An inductively-coupled plasma optical emission spectroscopy/mass spectrometry (ICP-OES/MS) was employed to analyze the chemical compositions of as-synthesized GQDs. X-ray photoelectron spectroscopy (XPS, Fison VG ESCA210) was adopted for characterizing the surface chemical composition of the samples. The sample preparation for the XPS measurement was also given in the ***Electronic*** ***Supporting Information*** (S1.2). The C 1s, N 1s and O 1s spectra were deconvoluted with a non-linear least square fitting algorithm written in-house (Note: the subroutine algorithm was based on the symmetric Gaussian function). The crystalline structure of GQD samples was analyzed using Raman spectroscopy (Renishaw Micro-Raman spectrometer). The sample preparation for TEM micrograph focusing on coronavirus attacked by GQDs was illustrated in the ***Electronic*** ***Supporting Information*** (S1.3).

Ultraviolet–visible (UV–vis) spectra of GQD suspensions were measured using an Agilent Cary 60 spectrometer (scan rate: 60 nm/min). To prepare the solutions, 200 mg of GQDs were dispersed within 1,000 mL of distilled water and were sonicated in water bath at ambient temperature for 20 min. To improve the GQD dispersibility, polyethylene glycol (PEG, molecular weight: 1,000) serving as the surfactant was also added to the GQD suspensions, where the ratio of PEG to GQD was set at 1:100 in w/w. Since the GQD samples were well dispersed in the polar solvents, the resulting suspensions were ultra-stable (>6 months). The GQD suspension was prepared with a concentration of 200 mg powder/1,000 mL distilled water within the quartz cells. A fluorescence spectrometer (Hitachi F-7000 FLS920P) was adopted to analyze the photoluminescence (PL) emission spectra. The PL measurements were performed excited at wavelengths of 360, 380, and 450 nm.

2.2.1. Cell viability and virus inhibition of functionalized GQDs

In this experiment, both H171 and H184 cells were used for the bio-compatibility analysis of the GQD solutions. A 96-well plate was employed for collecting the GQD samples of different concentrations and a 24-, 48-, and 72-h time frame was adopted to analyze the cell concentration. After that, the non-added sample was used as a control value to compare the cell viability. The related viability test for both H171 and H184 cells was repeated for three times. To explore the influence of GQD samples on the enveloped and non-enveloped viruses, FCoV NTU156 and EV71 were chosen as representatives for this work. Felis catus whole fetus-4 (Fcwf-4) cells for FCoV NTU156 [39] and human rhabdomyosarcoma (RD) cells for EV71 [40] were maintained in Dulbecco's Modified Eagle Medium with 10% fetal bovine serum, 100 IU/mL penicillin, and 100 IU/mL streptomycin solution in 5% CO_2 at 37 °C. RD cell is an immortalized cell line, which can support the growth of several avian viruses including the EV71.

The antiviral test of FCoV NTU156 by GQD sample was referred to the standard protocol outlined in the NF EN 14476 + A1 and ASTM E1053-97. After culturing feline coronavirus with Fcwf-4 cells, we prepared a 96-well plate of cells with 3×10^4 Fcwf-4 cells per well; and used>80% of the cells on the next day to determine the concentration of the virus. Next, 20 μL of FCoV NTU156 solution was placed into a 24-well plate and dried for 30 min. Followingly, 950 μL of cell culture and 50 μL GQD samples were added to these wells for 1, 5, and 10 min, and serially diluted the solution to perform an antiviral test. Cells infected with feline coronavirus underwent a 3-day incubation period and the cytopathic effect was recorded via crystal violet staining for median tissue culture infectious dose ($TCID_{50}$) assay. $TCID_{50}$ assay is usually considered an efficient method for verifying the viral titer of a testing virus, where the host tissue cells are cultured on a well plate titer, and then varying dilutions of the testing viral fluid are added to the wells. To assess the infectivity of the viruses, the following formula was used; infectivity % = (number of wells with virus-infected cells/number of wells with virus-inoculated cells) × 100%. Based on the infectivity percentages, the virus dilution can infect 50% of cells. $TCID_{50}$/mL was calculated as followed: ((infectivity % at dilution immediately above 50%) − 50%) / ((infectivity % at dilution immediately above 50%) / (infectivity % at dilution immediately below 50%)) [41].

For the EV71 antiviral test, the procedure was also based on the NF EN 14476 + A1 and ASTM E1053-97 standard test protocol. After culturing EV71 with RD cells, a 96-well plate of cells, 3×10^4 RD cells per well, was prepared and utilized more than 80% of the cells on the following day to quantify the virus level. Next, 20 μL of EV71 solution was poured into a 24-well plate, dried for 0.5 h, and then 950 μL of cell culture medium was added to the sample for 10 min, Finally, we serially diluted the solution to perform a virus potency test. The live cell staining was carried out with crystal violet to calculate $TCID_{50}$ value after three days (i.e., cell seeding).

To explore the efficacy of the GQD spray, the antiviral effect of GQD-coated glass substrate was also investigated. The test method was based on the ISO 21702:2019 standard procedure. Herein the GQD solution was homogeneously spread by a high-performance spin coater. The thickness of the GQD layer was controlled at ~ 200 μm. The GQD surface with the geometrical area of ~ 5 × 5 cm^2 was then placed in the vacuum oven and maintained at 70 °C for 6 h. The FCoV NTU156 virus was cultured with Fcwf-4 cells and was distributed on the GQD-coated glass surface to examine its anti-coronavirus characteristics. Here, a similar experimental apparatus (e.g., a 96-well plate with 3×10^4 Fcwf-4 cells) was adopted to determine the concentration of the virus within the test well. Followingly, 150 μL of the virus-containing solution was evenly spread on the glass surface of ~ 5 cm^2 for 8 and 20 h, respectively. Then, the surface was rinsed with 10 mL of the culture solution, and the resulting medium was serially diluted to perform a virus potency test. The live cell staining was performed with crystal violet to quantify the $TCID_{50}$ after three days of cell seeding. Herein the virus inhibition rate was assessed using the following formula: ["$TCID_{50}$/100 μL of the original virus solution" - "$TCID_{50}$/100 μL of the virus medium after adding the product"] / ["The original virus solution $TCID_{50}$/100 μL × 100%"].

3. Results and discussion

The optical images of different GQD samples in distilled water under the sunlight and blue light (wavelength: 450 nm) are shown in Fig. 1. According to Fig. 1, all the samples in water are transparent under the sunlight. However, under the blue-light illumination, the GQD suspensions illuminate yellow-green (GQD-1), green

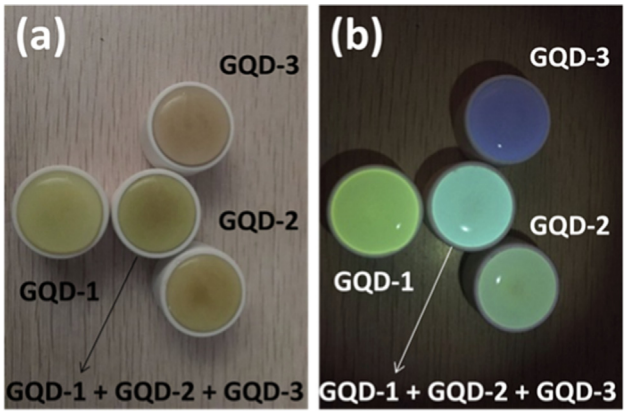

Fig. 1. Photographs of different GQD suspensions in distilled water under (a) sunlight and (b) blue light illumination (wavelength: 450 nm). (For interpretation of the references to colour in this figure legend, the reader is referred to the web version of this article.)

(GQD-2), and deep blue (GQD-3) in water and ethanol. Also, as shown in Fig. 1, the mixture of GQD-1 + GQD-2 + GQD-3 suspension is cyan under the blue-light source.

The PL emission spectra of GQD-3 suspension excited at different wavelengths are illustrated in the ***Electronic Supporting Information*** (see Figure S1(a)). The GQD-3 sample displays a quasi-symmetric peak ranging from 380 to 500 nm under 360- and 380-nm excitation, whereas an obvious red-shift to the wavelength range of 500–600 nm under blue light illumination. Apparently, the GQD-3 suspension exhibits tunable PL emission, where the wavelength-dependent PL response (i.e., red shift) in water can be presumably due to the thermal loss and/or the formation of excited-state relaxation channel [42].

Typical Raman spectra of GQD samples are depicted in Figure S1 (a), where three main peaks are identified: *D* band (*ca.* 1350 cm^{-1}), *G* band (*ca.* 1580 cm^{-1}), and 2*D* band (*ca.* 2700 cm^{-1}). The Raman band observed at 1580 cm^{-1} mainly originates from a single crystallite of graphite (*G* band). The *D* band at 1350 cm^{-1} is commonly attributed to amorphous carbon or deformation vibrations of a hexagonal ring [43–45] The intensity ratio of *D* to *G* bands (I_D/I_G) can be considered as an index of the graphitic degree of carbon-based materials [35]. After calculation, the I_D/I_G ratio shows an average of 0.94–0.97 for all samples. This result indicates that all GQD samples synthesized via the SPMA method possess a similar crystalline microstructure, demonstrating a non-detrimental influence of the precursor configuration (i.e., the weight ratio of citric acid to urea) on the crystallinity.

Fig. 2(a)- 2(c) include the HR-TEM micrographs of GQD samples. Based on Fig. 2, the GQDs form a quasi-spherical shape (i.e., circular (GQD-1) and elliptical (GQD-2 and GQD-3)) through the SPMA method. Herein the dashed white curves are used to outline the edges of the particles. Considering the lattice fringes developed on the GQD nanoparticles (see Fig. 2), superb crystallinity with a lattice distance of ~ 0.22 nm (corresponding to the (1120) lattice fringe of graphene-based materials [46]) can be observed for all the samples. The formation of the circular peripheries is majorly due to minimizing the edge free energy during the equilibrium state where the uncombined atoms (e.g., C, N, O) migrate to rearrange and subsequently reconstruct the crystal structure [47,48]. The corresponding particle size distributions of the particles are collected and shown in Fig. 1(d)- 1(f), where the GQD-1 configuration possesses the narrowest distribution and smallest average particle size among all the samples. The average nanoparticle sizes of the GQDs were ~ 3.3, 4.1, and 4.2 nm for the GQD-1, GQD-2, and GQD-3 samples, respectively.

To further characterize the surface chemistry, ICP-OES/MS and XPS analyses were performed to uncover the chemical composi-

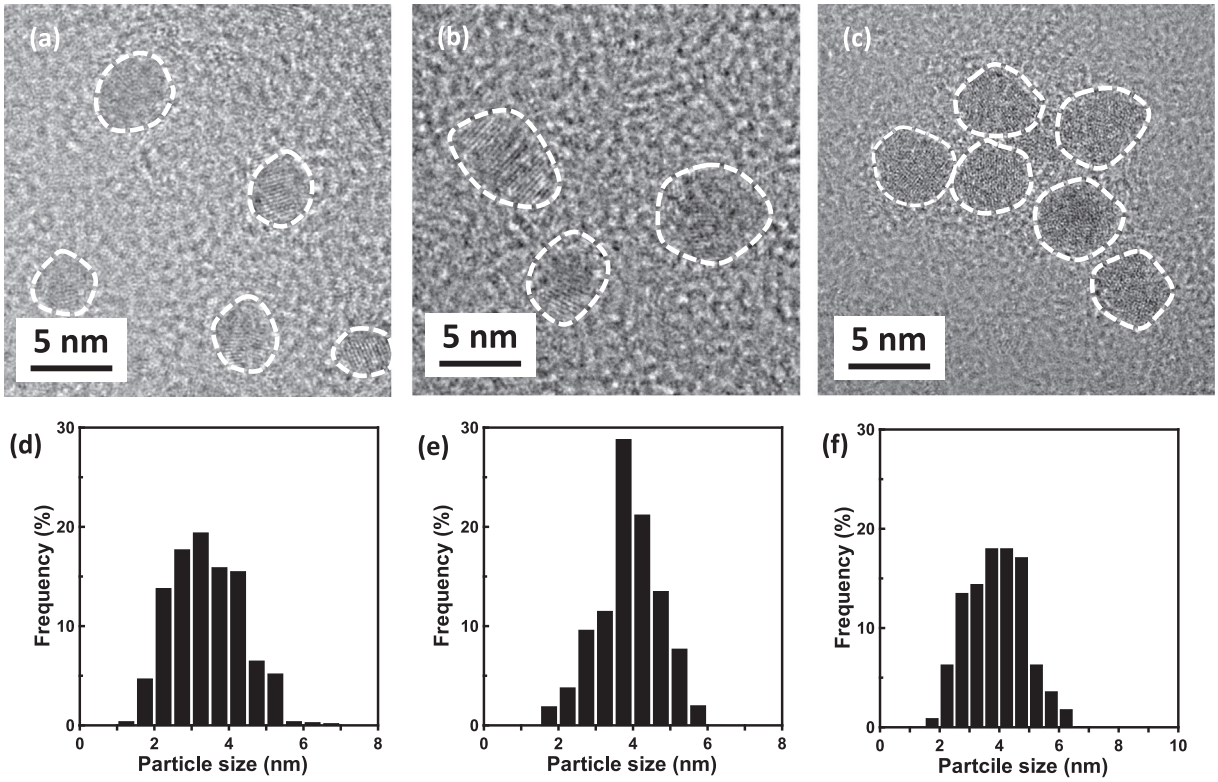

Fig. 2. HR-TEM micrographs of (a) GQD-1, (b) GQD-2, and (c) GQD-3 samples. Particle size distributions of (d) GQD-1, (e) GQD-2, and (f) GQD-3 samples.

tions of the as-synthesized GQD nanoparticles. Table 1 includes the oxidation and amidation levels of GQD samples, determined by the ICP-OES/MS. As tabulated in Table 1, the O/C ratio (i.e., oxidation level) is in the range of 56.2–65.0 at.% for the GQD samples, exhibiting highly-oxidized surface morphology (i.e., highly hydrophilic). The C 1s spectra can be decomposed into five peaks at 284.4 eV (C═C or C— C), 285.2 eV (C— N), 287.5 eV (C- OH), 288.5 (C═O), and 289.5 eV (O═C— OH), indicating different bonding types to the C atoms [36], as shown in Fig. 3(a). The presence of surface functionalities reveals that the resulting GQD samples con-

Table 1
Surface amidation/oxidation level and functional group distribution on functionalized GQD samples.

GQD type	O/C ratio	Phenolic	Carbonyl	Carboxylic
	(at.%)	(C-OH, %)	(C═O, %)	(O═C- OH, %).
GQD-1	61.1	11.1	23.7	65.2
GQD-2	56.2	51.3	37.6	11.1
GQD-3	65.0	42.3	49.1	8.6
GQD type	N/C ratio	N oxide	Quaternary N N	Pyrrolic + Pyridinic
	(at.%)	(%)	(%)	(%)
GQD-1	66.2	0	33.2	66.8
GQD-2	48.1	0	23.3	76.7
GQD-3	34.2	10.9	18.6	70.5

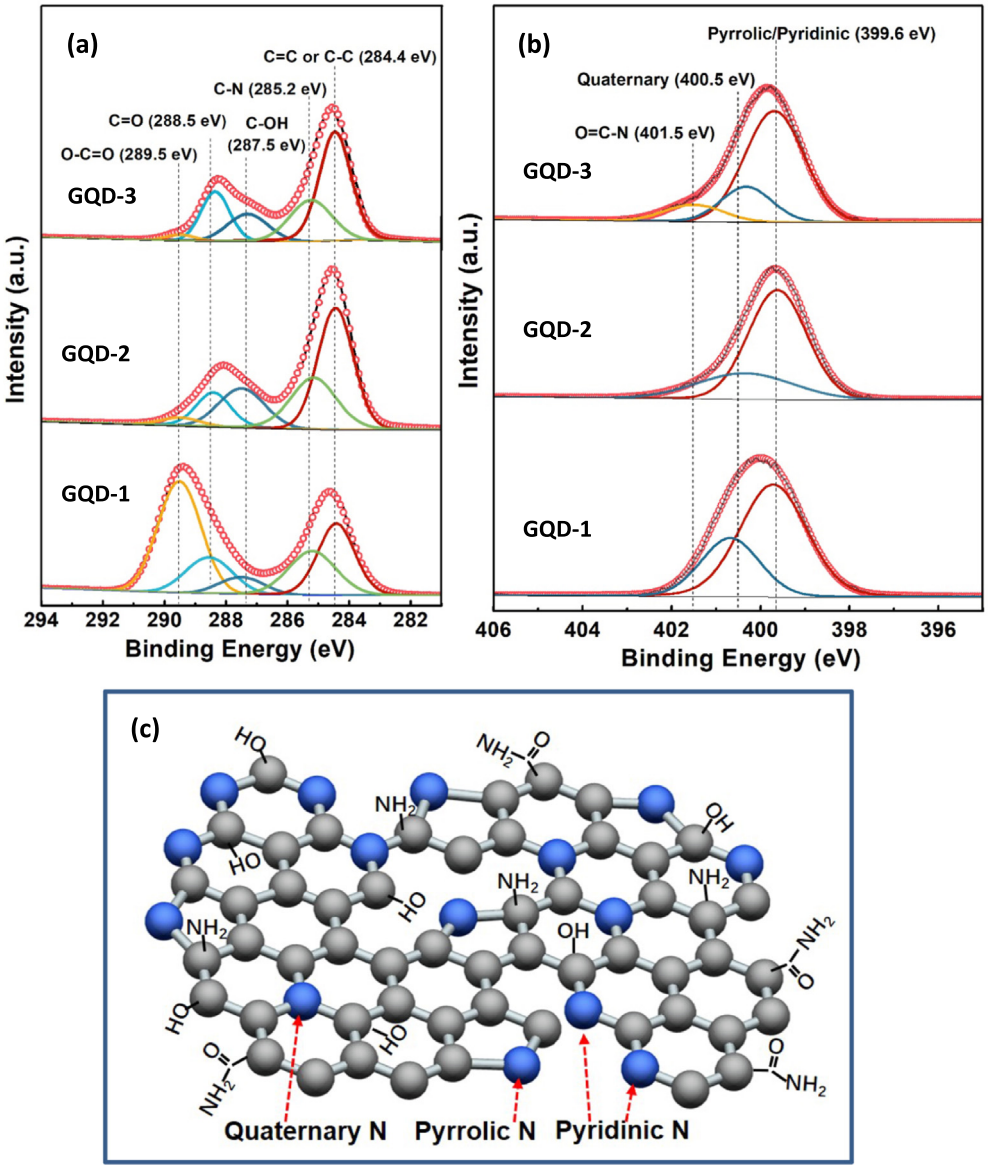

Fig. 3. Detailed-scan XPS (a) C 1s and (b) N 1s spectra of functionalized GQD samples. Schematic diagram of surface functionalities on GQD-3 sample, where the functional groups contain pyrrolic N, pyridinic N, graphitic N, amino group.

sist of *N*-doped graphene oxide ($C_xN_yO_z$) crystals. Table 1 also shows the N/C atomic ratio (i.e., amidation level) as an increasing function of the urea content within the precursor. The N/C atomic ratios of the GQD-1, GQD-2, and GQD-3 samples (see Table 1) are 66.2, 48.1, and 34.2 at.%, respectively (based on the analysis of the ICP-OES/MS). High-resolution N 1s XPS spectra (see Fig. 3(b)) can be deconvoluted into the signals with predominant pyrrolic or pyridinic N (*ca.* 399.6 eV), quaternary N (*ca.* 400.4 eV), and *N*-oxides (e.g., O═C- N) at *ca.* 401.5 eV [49,50]. The first component can be assigned to the presence of aromatic C═N—C, in which nitrogen bonds to two carbon atoms or pyridine moiety, while the second one corresponds to the tertiary N- $(C)_3$ that quaternary N is connected to three sp^2 carbon atoms, (i.e., graphitic nitrogen) [51,52]. The third peak represents the amino C—N—H group, mainly originates from the amide- carbonyl group (O═C- NH_2), e.g., amino and amide carbonyl functional groups, located at the edges of the graphene sheets [53,54]. As quantified in Table 1, all the GQD nanoparticles possess high amidation level, where the pyrrolic + pyridinic N is the major contributor for such an increase in amidation content. However, only GQD-3 sample contains 10.9% amide- carbonyl group attached to the edges of the graphene layer, as illustrated in Fig. 3(c).

The cell toxicity of GQD-1, GQD-2, and GQD-3 samples was established on H171 cell lines after 24, 48, and 72 h incubation. Fig. 4(a) shows the photographs of the cell viability in GQD-3 solution with different concentrations, ranging from 0.25 to 50 μg/mL. As illustrated in Fig. 4(a), it can be observed that the GQD-3 displays excellent bio-compatibility even at the highest concentration (i.e., 50 μg/mL), as compared to the control sample. According to Fig. 4(b), all GQDs are nontoxic towards H171 cells throughout the entire concentration range (0.25–50 μg/mL) with over 80% cell viability compared to control cells when incubated for 72 h; thus, they all have an adverse influence on the cell toxicity. To further analyze the bio-compatibility, Fig. 5 shows relative cell viability as a function of dilution of GQD-3 sample upon 72 h incubation with H184 (cell type) at 100 μg/mL. The trend shown in Fig. 5, also indicates an adequate cell viability for the GQD-3 sample towards H184 cell at different dilutions.

The viral infection inhibitions (i.e., FCoV NTU156) in the presence of different GQDs at various concentrations were also col-

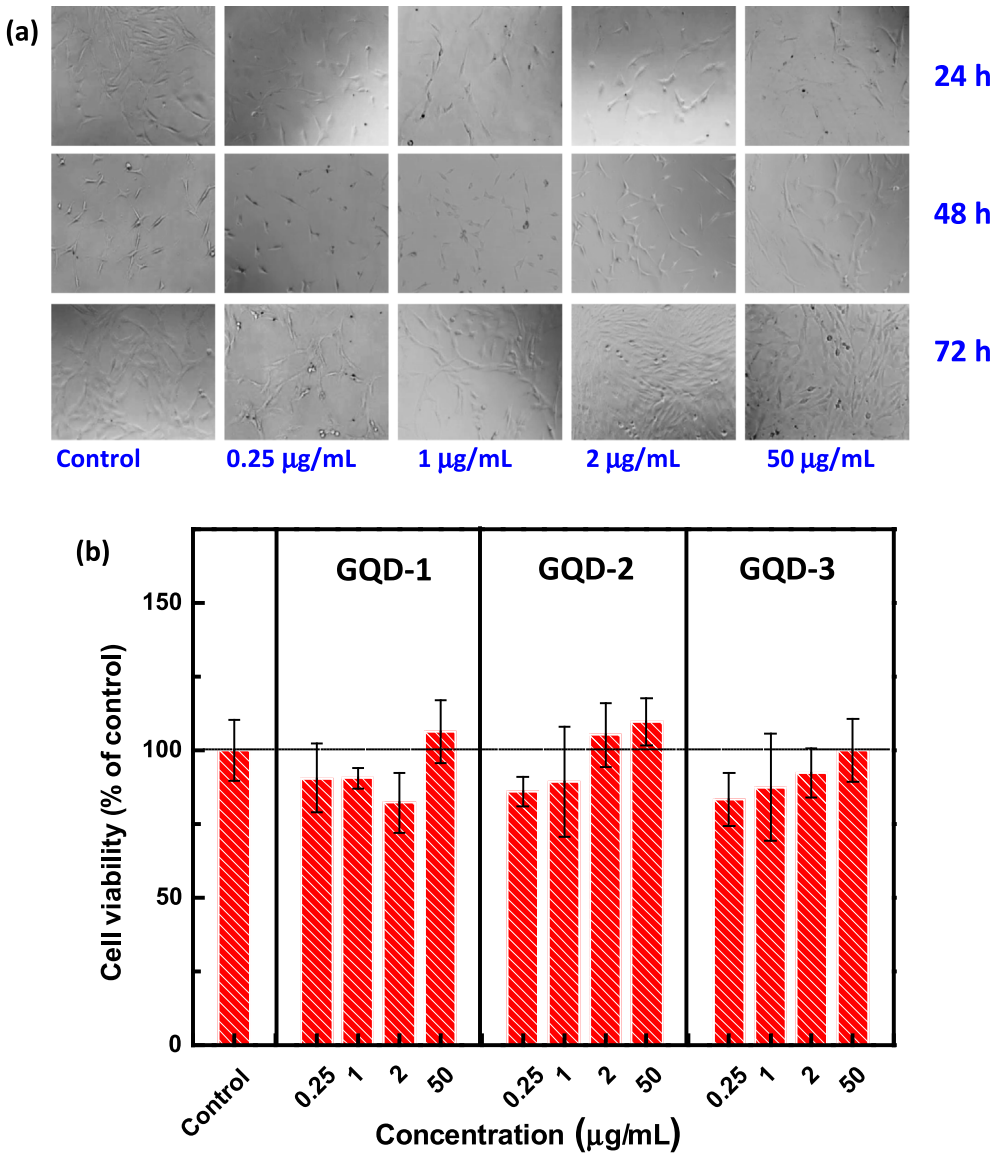

Fig. 4. (a) Optical images of cell viability at different GQD-3 concentrations for 24, 48, and 72 h, and (b) cell viability as function of GQD concentration after 72 h incubation (cell type: H171).

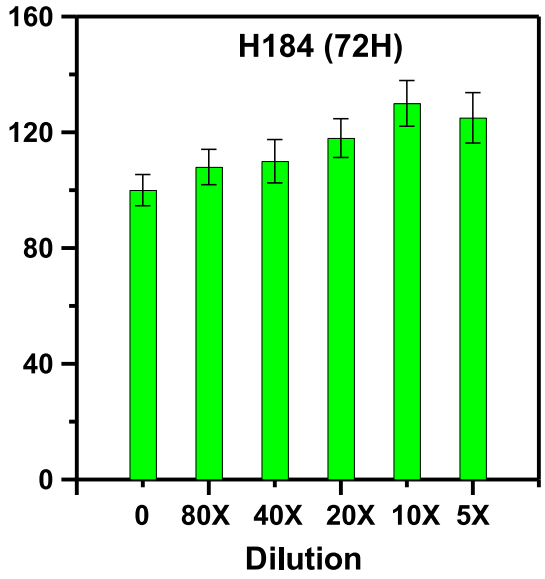

Fig. 5. Relative cell viability as a function of dilution of GQD-3 sample at 72 h incubation (cell type: H184; original concentration: 100 μg/mL).

lected, as summarized in Table 2. We observe that the addition of both GQD-1 and GQD-2 sample after ~ 5 min of infection with the virus, exhibits relatively low inhibition (~25.87%), indicating that these nanoparticles are partially interfering with the FCoV NTU 156 entry or replication. In contrast, GQD-3 sample not only displays better antiviral effect but also demonstrates a concentration-dependent virus inactivation. The effective concentration to achieve > 90% inhibition against FCoV NTU156 infection is ~ 10 mg/mL. This observation reveals that the GQD structure has a substantial influence on the antiviral performance, majorly due to various surface functionalization on the graphene surface. We note that GQD-3 nanomaterial contains a number of amide- carbonyl group (O=C- NH_2) and a significant amount of oxygen functionalities (e.g., phenolic and carbonyl groups) at the edge sites as well as the basal planes, favoring the interaction with S protein. It is postulated that molecular docking is an efficient approach for the prediction of the interaction of GQDs with the S protein of the coronavirus, which warrants further analysis to assess their potential applications as an antiviral agent [55]. The calculations of blind docking experiments can be performed with the Hex 8.0.0 program [55]. Previous studies have reported on the effectiveness of phenolic and amide- carbonyl groups, with binding energies of −699.3 and −592.2 kJ/mol and active site occupations of 80% and 85% on the coronavirus, respectively [55]. Among all the nanomaterials synthesized in this work, the GQD-3 sample provides high surface coverage (i.e., the percentage of phenolic and amino groups), capable of strongly interacting with the RBD of the S protein. Accordingly, functionalized GQDs are suitable scaffolds to interfere with the entry of viruses into the cells, leading to deactivation of the virus [56,57].

To inspect the antiviral mechanism triggered by the functionalized GQDs, HR-TEM micrographs were taken when the FCoV NTU156 was deactivated by GQD-3, as shown in Fig. 6. First, we observe that FCoV NTU156 possesses a round-like shape with an average diameter of ~ 80–100 nm, where a large amount of GQDs are attached to the surface of the virus due to the strong interaction between the surface functionalities and the S protein (see Fig. 6(a)). Second, the adsorbed GQDs hinder the virus infection at early stages through inhibiting the interaction of the protein S-receptor with the host cell membrane. Meanwhile, the S protein on the surface of the coronavirus can be sequestered or even disabled by the positive surface charge of the cationic GQDs [58]. Thus, the positive charge on the surface of GQD nanoparticles interact with the genome of the virus and triggers the generation of ROS within the virion, which impedes the negative strand RNA replication [59–61]. It is generally recognized that functionalized GQDs could generate singlet oxygen ($^1O_2$) under blue or white light irradiation, exhibiting pro-oxidant properties [62,63]. Meanwhile, both phenolic and amide- carbonyl groups are known to adsorb onto the lipid membrane wall, which provides the molecules bearing this functional groups are diffusing into the virus interior, where the disruption of the lipid membrane eventually leads to the virial destruction [15,64]. Since the antivirial test was carried out under visible light illumination, the action of GQD-3 sample on lipid membrane wall can be twofold: the generated singlet oxygen penetrates membrane wall and the functional groups adsorb on membrane wall, thus enabling GQDs to enter the virus and cause oxidative stress. As illustrated in Fig. 6(b), the round-like structural morphology of the virus is destroyed when the GQD nanoparticles penetrate through the virus surface partially prying apart the lipid membrane. Accordingly, the surface functionalities of the GQDs play a critical role in enhancing the antiviral activity of the GQDs towards the coronavirus.

Although the GQD-3 sample exhibits a relatively high inhibition rate (~96.61%) towards the FCoV NTU156 at 10 mg/mL, further improving the virus inhibition along with reducing the GQD dose

Table 2
Virus inhibition assay of the viruses incubated with functionalized GQD samples.

GQD sample	Concentration (mg/mL)	$TCID_{50}$/mL	Inhibition (%).
A. *Feline Coronavirus NTU156 (FCoV NTU156)*			
Control	———	$10^{4.80}$	———
GQD-1	10 (5 min)	$10^{4.67}$	25.87
GQD-2	10 (5 min)	$10^{4.67}$	25.87
GQD-3	10 (5 min)	$10^{3.80}$	90.00
GQD-3	10 (10 min)	$10^{3.33}$	96.61
B. *Feline Coronavirus NTU156 (FCoV NTU156)*			
Control	———	$10^{4.59}$	———
GQD-3/PEG	1 (5 min)	$10^{1.91}$	99.79
Control	———	$10^{4.00}$	———
GQD-3/PEG	1 (30 min)	$10^{0.47}$	99.97
C. *Feline Coronavirus NTU156 (FCoV NTU156)*			
Control	———	$10^{4.61}$	———
GQD-3/PEG/glass	——— (8 h)	$10^{2.50}$	99.22
GQD-3/PEG/glass	——— (20 h)	$10^{1.50}$	99.92
D. *Enterovirus 71 (EV71)*			
Control	———	$10^{9.70}$	———
GQD-3	10 (10 min)	$10^{4.43}$	99.99

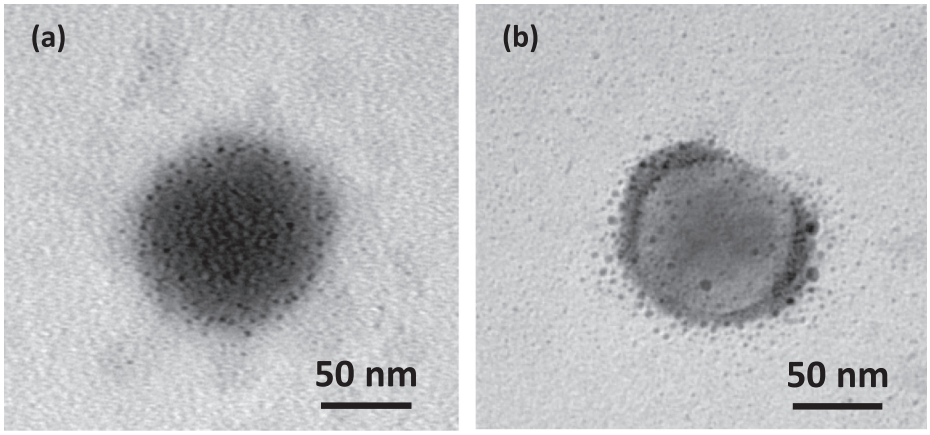

Fig. 6. HR-TEM micrograph of (a) GQDs adsorbed onto coronavirus and (b) GQD penetration through the virus, followed by prying it apart from lipid membrane.

is essential. To facilitate the attachment of GQD particles to the virus surface, PEG can be employed as a surfactant to disperse the GQDs within the aqueous solutions. Herein, the ratio of PEG to GQD-3 was adjusted at 1/100 in w/w. The addition of PEG polymer results in the partial coverage of the GQD surface, and enables the formation of a hydrophilic PEG skin layer due to the presence of $H-(O-CH_2-CH_2)_n-OH$ monomer [65]. It is also effective in constructing a three-dimensional domain capable of mitigating the GQD aggregation. The PEG layer facilitates the dispersion and the adsorption of functionalized GQDs onto the virus surface (i.e., enhancing the surface to volume ratio). As tabulated in Table 2 the inhibition of FCoV NTU156 reaches as high as 99.79% and 99.97% at 5 and 30 min, respectively. In addition, the GQD dose can be even reduced to 1 mg/mL, confirming that that the antiviral activity as well as the viral infection inhibition are significantly enhanced via addition of the PEG layer.

To explore the efficacy of functionalized GQDs against viral infection in realtime, a GQD-3 solution was uniformly sprayed on a glass substrate to characterize its antiviral effect. As quantified in Table 2 (see part (C)), the viral inhibition on GQD-coated glass reaches as high as 99.22% and 99.92% after 8 and 20 h, respectively. This finding demonstrates that functionalized GQD-coated surfaces maintain a long-term antiviral effect against the FCoV NTU156. Accordingly, we proposed a schematic diagram, as shown in Fig. 7, for describing a twofold plan (i.e., Plan (A) and (B)) of the anti-coronavirus mechanism being triggered in the presence of functionalized GQDs. The lipid membrane of the virus is destroyed in liquid phase (Plan (A)) and subsequently a GQD-coated protection layer is formed against the coronavirus (Plan (B)). Indeed, the functionalized GQDs interfere in early stages of infection and operate via altering the viral surface proteins. Next, the functional groups of the GQDs hinder the entrance of virus through generating a negative strand of RNA along with budding as a result of ROS accumulation in the presence of GQDs [66]. Due to this superior viral inhibition and enhanced bio-compatibility, functionalized GQDs can be uniformly sprayed on different substrates (e.g., textile, plastic, steel, wood, stone, and many others), as an inhibitor to combat the coronavirus.

To inspect the GQDs' effectiveness towards non-enveloped viruses, the antiviral effect of GQD samples was investigated via exposure to the EV71 virus (see part (D) in Table 2). As parametrized in Table 2, the inhibition of EV71 using as-synthesized GQD-3 reaches 99.99%. Therefore, the functionalized GQDs can be considered as a multisite inhibitor for not only the FCoV NTU156 but also for the EV71 virus. The nano-sized (average particle size: 4.2 nm) antiviral fluorescent GQDs with a positive charge

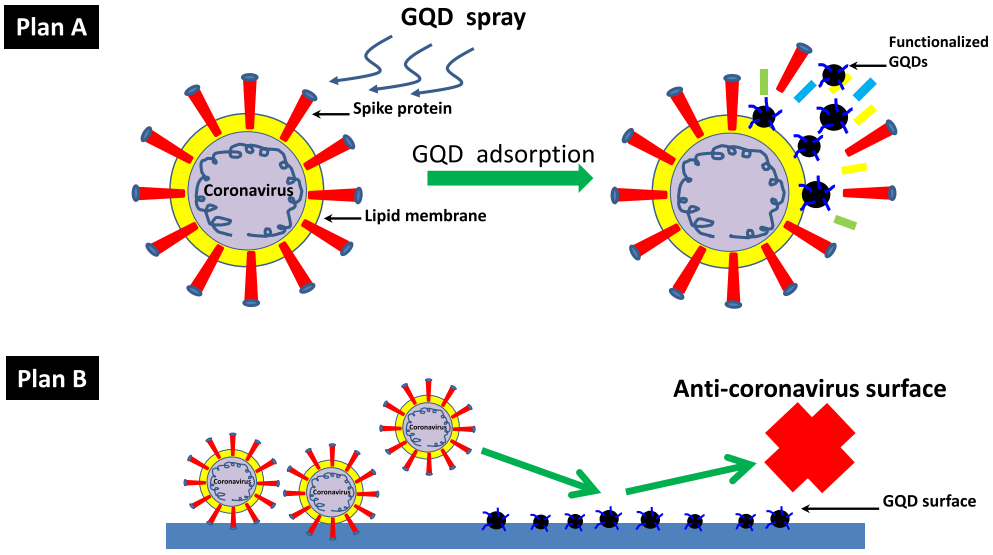

Fig. 7. Schematic diagram for describing two plans of anti-coronavirus effect in the presence of functionalized GQDs, where plan A and plan B represents destroying lipid membrane in liquid phase and generating GQD-coated protection layer against coronavirus, respectively.

and numerous hydrophilic functional groups implanted by the SPMA pyrolysis of citric acid + urea mixture are highly effective in combatting against enveloped and non-enveloped viruses.

4. Conclusions

In this work, antiviral GQD nanoparticles were synthesized through a novel SPMA method; and the as-synthesized GQDs were employed as high-performance inhibitor to combat the *Feline Coronavirus NTU156* (FCoV NTU156) and *Enterovirus 71* (EV71)) with exceptional inhibition (>99.9%). The SPMA technique is a facile and very efficient synthesis route for preparing *N*-functionalized GQDs at elevated temperatures (e.g., 280 °C). It was shown that the configuration of the N- and C-rich precursors significantly affects the chemical composition as well as the distribution of the oxygenated/nitrogenated functionalities on the resulting GQDs. The functionalized GQDs exhibited excellent biocompatibility according to the cell toxicity test of the H171 and H184 cells after 72 h incubation. It was shown that the surface functionality of the GQD nanoparticles play a critical role in enhancing the antiviral effect against the FCoV NTU156. Higher surface coverage with the phenolic and amino groups was found to be extremely advantageous for increasing the interactions with the receptor-binding-domain of the spike protein. Accordingly, functionalized GQDs are suitable scaffolds capable of interfering with the entry of coronavirus into the cells, leading to virus inactivation. To further improve the viral inhibition, the addition of PEG polymer was explored as an ultra-efficient strategy in facilitating the dispersion as well as the adsorption of the GQDs onto the virus surface. The efficacy of the functionalized GQD nanomaterials as ultra-efficient inhibitor to combat the coronavirus was confirmed via exposing a GQD-coated glass to this enveloped virus for a relatively long period (20 h). Due to remarkable viral inhibition and enhanced human cell's bio-compatibility, the functionalized GQDs developed in this work can be sprayed on different substrates as disinfectant to protect against various enveloped viruses (e.g., coronavirus).

CRediT authorship contribution statement

Chien-Te Hsieh: Methodology, Validation, Funding acquisition, Supervision, Writing – original draft, Writing – review & editing. **Siyong Gu:** Data curation, Methodology, Visualization, Investigation. **Yasser Ashraf Gandomi:** Validation, Writing – original draft, Writing – review & editing. **Chun-Chieh Fu:** Data curation, Investigation. **Po-Yu Sung:** Data curation, Visualization. **Ruey-Shin Juang:** Supervision, Validation, Conceptualization, Methodology, Writing – review & editing. **Cheng-Cheung Chen:** Methodology, Validation, Funding acquisition, Investigation, Writing – review & editing.

Data availability

No data was used for the research described in the article.

Declaration of Competing Interest

The authors declare that they have no known competing financial interests or personal relationships that could have appeared to influence the work reported in this paper.

Acknowledgments

The authors acknowledge the support of the Ministry of Science and Technology in Taiwan through grant numbers: MOST 108-2221-E-155-036-MY3, MOST 110-2623-E-006-002, MOST 111-2221-E-155-004, and MOST 109-2221-E-155-013. The authors also thank for antiviral test from Prof. Yi-Ning Chen (Department of Bioscience Technology, Chung Yuan Christian University, Taoyuan 32023, Taiwan). Partial financial support from Gold Carbon Inc. (Taiwan) is also appreciated.

Appendix A. Supplementary data

Supplementary data to this article can be found online at https://doi.org/10.1016/j.jcis.2022.10.082.

References

[1] A. Łoczechin, K. Séron, A. Barras, E. Giovanelli, S. Belouzard, Y.-T. Chen, et al., Functional carbon quantum dots as medical countermeasures to human coronavirus, ACS Appl. Mater. Interfaces 11 (2019) 42964–42974.
[2] S. Jindal, P. Gopinath, Nanotechnology based approaches for combatting COVID-19 viral infection, Nano Express 1 (2020) 022003.
[3] V. Palmieri, M. Papi, Can graphene take part in the fight against COVID-19?, Nano Today 33 (2020) 100883
[4] S. Manivannan, K. Ponnuchamy, Quantum dots as a promising agent to combat COVID-19, Appl. Organomet. Chem. e5887 (2020) 1–6.
[5] B. Udugama, P. Kadhiresan, H.N. Kozlowski, A. Malekjahani, M. Osborne, V.Y.C. Li, et al., Diagnosing COVID-19: the disease and tools for detection, ACS Nano 14 (2020) 3822–3835.
[6] S. Rosales-Mendoza, V.A. Márquez-Escobar, O. González-Ortega, R. Nieto-Gómez, J.I. Arévalo-Villalobos, What does plant-based vaccine technology offer to the fight against COVID-19?, Vaccine 8 (2020) 183
[7] C. Weiss, M. Carriere, L. Fusco, I. Capua, J.A. Regla-Nava, M. Pasquali, et al., Toward nanotechnology-enabled approaches against the COVID-19 pandemicm, ACS Nano 14 (2020) 6383–6406.
[8] S. Jiang, C. Hillyer, L. Du, Neutralizing antibodies against SARS-CoV-2 and other human coronaviruses, Trends Immunol. 41 (2020) 355–359.
[9] T. Magrone, M. Magrone, E. Jirillo, Focus on receptors for coronaviruses with special reference to angiotensin converting enzyme 2 as a potential drug target-a perspective, Endocr. Metab. Immune. Disord. Drug, Targets 20 (2020) 807–811.
[10] A.S. Galabov, Virucidal agents in the eve of manorapid synergy, GMS Krankenhhyg Interdiszip 2 (2007) 1–8.
[11] S.T. Jones, How materials can beat a virus, J. Mater. Sci. 55 (2020) 9148–9151.
[12] M. Zare, M. Sillanpää, S. Ramakrishna, Essential role of quantum science and nanoscience in antiviral strategies for COVID, Adv. Mater. 2 (2021) 2188–2199.
[13] Z.M. Markovic, B.Z. Ristic, K.M. Arsikin, D.G. Klisic, L.M. Harhaji-Trajkovic, B.M. Todorovic-Markovic, D.P. Kepic, T.K. Kravic-Stevovic, S.P. Jovanovic, M.M. Milenkovic, D.D. Milivojevic, V.Z. Bumbasirevic, M.D. Dramicanin, V.S. Trajkovic, Graphene quantum dots as autophagy-inducing photodynamic agents, Biomaterials 33 (2021) 7084–7092.
[14] B.Z. Ristic, M.M. Milenkovic, I.R. Dakic, B.M. Todorovic-Markovic, M.S. Milosavljevic, M.D. Budimir, V.G. Paunovic, M.D. Dramicanin, Z.M. Markovic, V.S. Trajkovic, Photodynamic antibacterial effect of graphene quantum dots, Biomaterials 35 (2014) 4428–4435.
[15] Z.M. Marković, S.P. Jovanović, P.Z. Mašković, M. Danko, M. Mičušík, V.B. Pavlović, D.D. Milivojević, A. Kleinová, Z. Špitalský, B.M.T. Marković, Photo-induced antibacterial activity of four graphene based nanomaterials on a wide range of bacteria, RSC Adv. 8 (2018) 31337–31347.
[16] Z. Luo, D. Yang, C. Yang, X. Wu, Y. Hu, Y. Zhang, L. Yuwen, E.K.L. Yeow, L. Weng, W. Huang, L. Wang, Graphene quantum dots modified with adenine for efficient two-photon bioimaging and white light-activated antibacterial, Appl. Surf. Sci. 434 (2018) 155–162.
[17] Y. Zhang, C. Yang, D. Yang, Z. Shao, Y. Hu, J. Chen, L. Yuwen, L. Weng, Z. Luo, L. Wang, Reduction of graphene oxide quantum dots to enhance the yield of reactive oxygen species for photodynamic therapy, Phys. Chem. Chem. Phys. 20 (2018) 17262–17267.
[18] V. Volarevic, V. Paunovic, Z. Markovic, B.S. Markovic, M. Misirkic-Marjanovic, B. Todorovi-Markovi, S. Bojic, L. Vucicevic, S. Jovanovic, N. Arsenijevic, I. Holclajtner-Antunovi, M. Milosavljevic, M. Dramicanin, T. Kravic-Stevovic, D. Ciric, M.L. Lukic, V. Trajkovic, Large graphene quantum dots alleviate immune-mediated liver damage, ACS Nano 8 (2014) 12098–12109.
[19] Z.M. Marković, S.P. Jovanović, P.Z. Mašković, M.M. Mojsin, M.J. Stevanović, M. Danko, M. Mičušík, D.J. Jovanović, A. Kleinová, Z. Špitalský, V.B. Pavlović, B.M.T. Marković, Graphene oxide size and structure pro-oxidant and antioxidant activity and photoinduced cytotoxicity relation on three cancer cell lines, J. Photochem. Photobiol. B: Biol. 200 (2019) 111647.
[20] H. Sun, L. Wu, W. Wei, X. Qu, Recent advances in graphene quantum dots for sensing, Mater. Today 16 (2013) 433–442.
[21] R.-S. Juang, C.-T. Hsieh, C.-P. Kao, Y. Ashraf Gandomi, C.-C. Fu, S.-H. Liu, et al., Highly fluorescent green and red emissions from boron-doped graphene quantum dots under blue light illumination 176 (2021) 61–70.
[22] H.M.R. Gonçalves, A.J. Duarte, J.C.G. Esteves Da Silva, Optical fiber sensor for Hg (II) based on carbon dots, Biosens. Bioelectron. 26 (2010) 1302–1306.

[23] S. Gu, C.-T. Hsieh, Y.-Y. Tsai, Y. Ashraf Gandomi, S. Yeom, K.D. Kihm, et al., Sulfur and nitrogen co-doped graphene quantum dots as a fluorescent quenching probe for highly sensitive detection toward mercury ions, ACS Appl. Nano Mater. 2 (2019) 790–798.
[24] S. Yang, L. Cao, P.G. Luo, F. Lu, X. Wang, H. Wang, et al., Carbon dots for optical imaging in vivo, J. Am. Chem. Soc. 131 (2009) 11308–11309.
[25] C.-C. Fu, C.-Y. Wu, C.-C. Chien, T.-H. Hsu, S.-F. Ou, S.-T. Chen, et al., Polyethylene $glycol_{6000}$/carbon nanodots as fluorescent bioimaging agents, Nanomaterials 10 (2020) 677.
[26] S. Gu, C.-T. Hsieh, B.C. Mallick, C.-C. Fu, R.-S. Juang, Y. Ashraf Gandomif, et al., Novel electrochemical sensor based on highly amidized graphene quantum dots to electrochemically detect hydrogen peroxide, Appl. Surf. Sci. 528 (2020) 146936.
[27] S. Gu, C.-T. Hsieh, B.C. Mallick, Y. Ashraf Gandomi, Infrared-assisted synthesis of highly amidized graphene quantum dots as metal-free electrochemical catalysts, Electrochim. Acta 360 (2020) 137009.
[28] D. Chao, C. Zhu, X. Xia, J. Liu, X. Zhang, J. Wang, et al., Graphene quantum dots coated VO_2 arrays for highly durable electrodes for Li and Na ion batteries, Nano Lett. 15 (2015) 565–573.
[29] L. Ruiyi, J. Yuanyuan, Z. Xiaoyan, L. Zaijun, G. Zhiguo, W. Guangli, et al., significantly enhanced electrochemical performance of lithium titanate anode for lithium ion battery by the hybrid of nitrogen and sulfur co-doped graphene quantum dots, Electrochim. Acta 178 (2015) 303–311.
[30] S. Gu, T. Christensen, C.-T. Hsieh, B.C. Mallick, Y. Ashraf Gandomi, J. Li, et al., Improved lithium storage capacity and high rate capability of nitrogen-doped graphite-like electrode materials prepared from thermal pyrolysis of graphene quantum dots, Electrochim. Acta 354 (2020) 136642.
[31] M.C. Daugherty, S. Gu, D.S. Aaron, B.C. Mallick, Y. Ashraf Gandomi, C.-T. Hsieh, Decorating sulfur and nitrogen co-doped graphene quantum dots on graphite felt as high-performance electrodes for vanadium redox flow batteries, J. Power Sources 477 (2020) 228709.
[32] Y. Wang, A. Hu, Carbon quantum dots: synthesis, properties and applications, J. Mater. Chem. C 2 (2014) 6921–6939.
[33] S. Miao, K. Liang, J. Zhu, B. Yang, D. Zhao, B. Kong, Hetero-atom-doped carbon dots: doping strategies, properties and applications, Nano Today 33 (2020) 100879.
[34] P. Garga, S. Sangama, D. Kochhar, S. Paharic, C. Kar, M. Mukherjee, Exploring the role of triazole functionalized heteroatom co-doped carbon quantum dots against human coronaviruses, Nano Today 35 (2020) 101001.
[35] S. Gu, C.-T. Hsieh, Y. Ashraf Gandomi, J.-K. Chang, J. Li, J. Li, et al., Microwave growth and tunable photoluminescence of nitrogen-doped graphene and carbon nitride quantum dots, J. Mater. Chem. C 7 (2019) 5468–5476.
[36] S. Gu, C.-T. Hsieh, Y. Ashraf Gandomi, J. Li, X.X. Yue, J.-K. Chang, Tailoring fluorescence emissions, quantum yields, and white light emitting from nitrogen-doped graphene and carbon nitride quantum dots, Nanoscale 11 (2019) 16553–16561.
[37] Y.-N. Chen, Y.-H. Hsueh, C.-T. Hsieh, D.-Y. Tzou, P.-L. Chang, Antiviral activity of graphene-silver nanocomposites against non-enveloped and enveloped viruses, Int. J. Environ. Res. Public Health 13 (2016) 430.
[38] J.-R. Wang, Y.-C. Tuan, H.-P. Tsai, J.-J. Yan, C.-C. Liu, I.-J. Su, Change of major genotype of entrovirus 71 in outbreaks of hand-foot-and-mouth disease in Taiwan between 1998 and 2000, J. Clin. Microbiol. 40 (2002) 10–15.
[39] N.C. Pedersen, J.W. Black, J.F. Boyle, J.F. Evermann, A.J. McKeirnan, R.L. Ott, Pathogenic differences between various feline coronavirus isolates, Adv. Exp. Med. Biol. 173 (1984) 365–380.
[40] J. Lu, Y.-Q. He, L.-N. Yi, H. Zan, H.-F. Kung, M.-L. He, Viral kinetics of enterovirus 71 in human abdomyosarcoma cells, World J. Gastroenterol. 17 (2011) 4135–4142.
[41] L.J. Reed, H. Muench, A simple method of estimating fifty percent endpoints, Am. J. Epidemiol. 27 (1938) 493–497.
[42] S. Kim, S.W. Hwang, M.K. Kim, Y.S. Dong, H.S. Dong, O.K. Chang, S.B. Yang, J.H. Park, E. Hwang, S.H. Choi, Anomalous behaviors of visible luminescence from graphene quantum dots: interplay between size and shape, ACS Nano 6 (2012) 8203–8208.
[43] Y.T. Lee, N.S. Kim, J. Park, J.B. Han, Y.S. Choi, H. Ryu, H.J. Lee, Temperature-dependent growth of carbon nanotubes by pyrolysis of ferrocene and acetylene in the range between 700 and 1000°C, Chem. Phys. Lett. 372 (2003) 853–859.
[44] K. Kim, K. Kim, W.S. Jung, S.Y. Bae, J. Park, J. Choi, J. Choo, Investigation on the temperature-dependent growth rate of carbon nanotubes using chemical vapor deposition of ferrocene and acetylene, Chem. Phys. Lett. 401 (2005) 459–464.
[45] L. Ni, K. Kuroda, L. Zhou, T. Kizuka, K. Ohta, K. Matsuishi, J. Nakamura, Kinetic study of carbon nanotube synthesis over Mo/Co/MgO catalysts, Carbon 44 (2006) 2265–2272.
[46] J. Peng, W. Gao, B.K. Gupta, Z. Liu, R. Romero-Aburto, L. Ge, et al., Graphene quantum dots derived from carbon fibers, Nano Lett. 12 (2012) 844–849.
[47] T. Xu, K. Yin, X. Xie, L. He, B. Wang, L. Sun, Size-dependent evolution of graphene nanopores under thermal excitation, Small 8 (2012) 3422–3426.
[48] X. Jia, M. Hofmann, V. Meunier, B.G. Sumpter, J. Campos-Delgado, J.M. Romo-Herrera, Controlled formation of sharp zigzag and armchair edges in graphitic nanoribbons, Science 323 (2009) 1701–1705.
[49] Y. Dai, H. Long, X. Wang, Y. Wang, Q. Gu, W. Jiang, et al., Doping: versatile graphene quantum dots with tunable nitrogen doping, Part. Part. Syst. Char. 31 (2014) 597–604.
[50] S. Barman, M. Sadhukhan, Facile bulk production of highly blue fluorescent graphitic carbon nitride quantum dots and their application as highly selective and sensitive sensors for the detection of mercuric and iodide ions in aqueous media, J. Mater. Chem. 22 (2012) 21832–21837.
[51] K. Chen, Z. Chai, C. Li, L. Shi, M. Liu, Q. Xie, et al., Catalyst-free growth of three-dimensional graphene flakes and graphene/g-C_3N_4 composite for hydrocarbon oxidation, ACS Nano 10 (2016) 3665–3673.
[52] A. Wang, C. Wang, L. Fu, W. Wong-Ng, Y. Lan, Recent advances of graphitic carbon nitride-based structures and applications in catalyst, sensing, imaging, and LEDs, Nano-Micro Lett. 9 (2017) 47.
[53] G.S. Kumar, R. Roy, D. Sen, U.K. Ghorai, R. Thapa, N. Mazumder, et al., Amino-functionalized graphene quantum dots: origin of tunable heterogeneous photoluminescence, Nanoscale 6 (2014) 3384–3391.
[54] C.T. Hsieh, C.Y. Lin, Y.F. Chen, J.S. Lin, H. Teng, Silver nanorods attached to graphene sheets as anode materials for lithium-ion batteries, Carbon 62 (2013) 109–116.
[55] Z. Ramezani, M.R. Dayer, S. Noorizadeh, M. Thompson, Deactivation of SARS-CoV-2 via shielding of spike glycoprotein using carbon quantum dots: bioinformatic perspective, COVID 1 (2021) 120–129.
[56] A. Barras, Q. Pagneux, F. Sane, Q. Wang, R. Boukherroub, D. Hober, et al., High efficiency of functional carbon nanodots as entry inhibitors of herpes simplex virus type 1, ACS Appl. Mater. Interfaces 8 (2016) 9004–9013.
[57] T. Du, J. Liang, N. Dong, L. Liu, L. Fang, S. Xiao, et al., Carbon dots as inhibitors of virus by activation of type I interferon response, Carbon 110 (2016) 278–285.
[58] D. Ting, N. Dong, L. Fang, J. Lu, J. Bi, S. Xiao, et al., Multisite inhibitors for enteric coronavirus: antiviral cationic carbon dots based on curcumin, ACS Appl. Nano Mater. 1 (2018) 5451–5459.
[59] X. Dong, M.M. Moyer, F. Yang, Y.P. Sun, L. Yang, Carbon dots' antiviral functions against noroviruses, Sci. Rep. 7 (2017) 519.
[60] L. Chen, J. Liang, An overview of functional nanoparticles as novel emerging antiviral therapeutic agents, Mater. Sci. Eng. C 112 (2020) 110924.
[61] T. Tong, H. Hu, J. Zhou, S. Deng, X. Zhang, W. Tang, L. Fang, S. Xiao, Glycyrrhizic-acid-based carbon dots with high antiviral activity by multisite inhibition mechanisms, Small 16 (2020) 1906206.
[62] S. Liu, T.H. Zeng, M. Hofmann, E. Burcombe, J. Wei, R. Jiang, J. Kong, Y. Chen, Antibacterial activity of graphite, graphite oxide, graphene oxide, and reduced graphene oxide: membrane and oxidative stress, ACS Nano 5 (2011) 6971–6980.
[63] Y. Wang, W. Kong, L. Wang, J.Z. Zhang, Y. Li, X. Liu, Y. Li, Optimizing oxygen functional groups in graphene quantum dots for improved antioxidant mechanism, Phys. Chem. Chem. Phys. 21 (2019) 1336–1343.
[64] N.A. Travlou, D.A. Giannakoudakis, M. Algarra, A.M. Labella, E. Rodríguez-Castellón, T.J. Bandosz, S- and N-doped carbon quantum dots: Surface chemistry dependent antibacterial activity, Carbon 135 (2018) 104–111.
[65] R.-S. Juang, C.-C. Fu, C.-T. Hsieh, S. Gu, Y. Ashraf Gandomi, S.-H. Liu, Highly luminescent aggregate-induced emission from polyethylene glycol-coated carbon quantum dot clusters under blue light illumination, J. Mater. Chem. C 8 (2020) 16569–16576.
[66] S. Kotta, H.M. Aldawsari, S.M. Badr-Eldin, N.A. Alhakamy, S. Md, A.B. Nair, et al., Exploring the potential of carbon dots to combat COVID-19, Front. Mol. Biosci. 7 (2020) 616575 (1-11).